Massive crossover elevation via combination of *HEI10* and *recq4a recq4b* during *Arabidopsis* meiosis

Heïdi Serra[a], Christophe Lambing[a], Catherine H. Griffin[a], Stephanie D. Topp[a], Divyashree C. Nageswaran[a], Charles J. Underwood[a,1], Piotr A. Ziolkowski[a,2], Mathilde Séguéla-Arnaud[b], Joiselle B. Fernandes[b,c], Raphaël Mercier[b], and Ian R. Henderson[a,3]

[a]Department of Plant Sciences, University of Cambridge, CB2 3EA Cambridge, United Kingdom; [b]Institute Jean-Pierre Bourgin (IJPB), Institut National de la Recherche Agronomique, AgroParisTech, CNRS, Université Paris-Saclay, 78000 Versailles, France; and [c]Université Paris-Sud, Université Paris-Saclay, 91405 Orsay, France

Edited by R. Scott Hawley, Stowers Institute for Medical Research, Kansas City, MO, and approved January 26, 2018 (received for review July 24, 2017)

During meiosis, homologous chromosomes undergo reciprocal crossovers, which generate genetic diversity and underpin classical crop improvement. Meiotic recombination initiates from DNA double-strand breaks (DSBs), which are processed into single-stranded DNA that can invade a homologous chromosome. The resulting joint molecules can ultimately be resolved as crossovers. In *Arabidopsis*, competing pathways balance the repair of ∼100–200 meiotic DSBs into ∼10 crossovers per meiosis, with the excess DSBs repaired as noncrossovers. To bias DSB repair toward crossovers, we simultaneously increased dosage of the procrossover E3 ligase gene *HEI10* and introduced mutations in the anticrossovers helicase genes *RECQ4A* and *RECQ4B*. As *HEI10* and *recq4a recq4b* increase interfering and noninterfering crossover pathways, respectively, they combine additively to yield a massive meiotic recombination increase. Interestingly, we also show that increased *HEI10* dosage increases crossover coincidence, which indicates an effect on interference. We also show that patterns of interhomolog polymorphism and heterochromatin drive recombination increases distally toward the subtelomeres in both *HEI10* and *recq4a recq4b* backgrounds, while the centromeres remain crossover suppressed. These results provide a genetic framework for engineering meiotic recombination landscapes in plant genomes.

meiosis | crossover | recombination | HEI10 | RECQ4

Meiosis is a conserved cell division required for eukaryotic sexual reproduction, during which a single round of DNA replication is coupled to two rounds of chromosome segregation, generating haploid gametes (1). Homologous chromosomes pair and recombine during prophase of the first meiotic division, which can result in reciprocal exchange, termed crossover (1). Crossovers have a major effect on sequence variation in populations and create genetic diversity. Meiotic recombination is also an important tool used during crop breeding to combine beneficial variants. However, crossover numbers are typically low, for example, approximately one to two per chromosome per meiosis, and can show restricted chromosomal distributions, which limits crop improvement. For example, recombination is suppressed in large regions surrounding the centromeres of many crop species (2). In this work we sought to use our understanding of meiotic recombination pathways to genetically engineer highly elevated crossover levels in *Arabidopsis*.

Meiotic recombination initiates from DNA double-strand breaks (DSBs), induced by SPO11 transesterases, which act in topoisomerase VI-like complexes (1) (*SI Appendix*, Fig. S1*A*). During catalysis, SPO11 becomes covalently bound to target site DNA (3). In budding yeast, SPO11 is then liberated by endonucleolytic cleavage by the MRX (Mre11–Rad50–Xrs2) complex and Sae2/COM1 (4–6). Simultaneously, exonucleases (Mre11 and Exo1) generate 3′-overhanging single-stranded DNA (ssDNA), hundreds to thousands of nucleotides in length (7, 8). Resected ssDNA is bound by RAD51 and DMC1 RecA-like proteins, which promote invasion of a homologous chromosome and the formation of a displacement loop (D loop) (9) (*SI Appendix*, Fig. S1*A*). Stabilization of the D loop can occur by template-driven DNA synthesis from the invading 3′ end (10) (*SI Appendix*, Fig. S1*A*). Strand invasion intermediates may then progress to second-end capture and formation of a double Holliday junction (dHJ), which can be resolved as a crossover or noncrossover, or undergo dissolution (1, 10) (*SI Appendix*, Fig. S1*A*).

The conserved ZMM pathway acts to promote formation of ∼85% of crossovers in plants, which are known as class I (1, 10) (*SI Appendix*, Fig. S1*A*). Mutations in ZMM genes severely reduce *Arabidopsis* crossover frequency, causing univalent chromosome segregation at anaphase I, aneuploid gametes, and infertility (1). Importantly, ZMM-dependent crossovers show interference, where double crossover (DCO) events are spaced out more widely than expected by chance (11, 12). The ZMM pathway in plants includes the MSH4/MSH5 MutS-related heterodimer, MER3 DNA helicase, SHORTAGE OF CROSSOVERS1 (SHOC1) XPF nuclease, PARTING DANCERS (PTD), ZIP4/SPO22, HEI10 E3 ligase, and

Significance

The majority of eukaryotes reproduce sexually, creating genetic variation within populations. Sexual reproduction requires gamete production via meiotic cell division. During meiosis, homologous chromosomes pair and undergo exchange, called crossover. Crossover is vital for crop breeding and remains a major tool to combine useful traits. Despite the importance of crossovers for breeding, their levels are typically low, with one to two forming per chromosome, irrespective of physical chromosome size. Here we genetically engineer superrecombining *Arabidopsis*, via boosting the major procrossover pathway (using additional copies of the *HEI10* E3-ligase gene), and simultaneously removing a major anti-recombination pathway (using mutations in *RECQ4A* and *RECQ4B* helicase genes). This strategy has the potential to drive massive crossover elevations in crop genomes and accelerate breeding.

Author contributions: H.S., C.L., C.H.G., D.C.N., R.M., and I.R.H. designed research; H.S., C.L., C.H.G., S.D.T., and D.C.N. performed research; C.J.U., P.A.Z., M.S.-A., and J.B.F. contributed new reagents/analytic tools; H.S., C.L., C.H.G., S.D.T., D.C.N., and I.R.H. analyzed data; and H.S., C.L., C.H.G., R.M., and I.R.H. wrote the paper.

Conflict of interest statement: The use of HEI10 to increase meiotic recombination is claimed in UK patent application number GB1620641.9 filed December 5, 2016, by the University of Cambridge. Patents were deposited by Institut National de la Recherche Agronomique on the use of RECQ4 to manipulate meiotic recombination in plants (EP3149027).

This article is a PNAS Direct Submission.

Data deposition: FastQ sequencing data have been deposited in the ArrayExpress database, https://www.ebi.ac.uk/arrayexpress/ (accession no. E-MTAB-5949).

[1]Present address: Vegetable Crop Research, KeyGene, 6708 PW Wageningen, The Netherlands.

[2]Present address: Department of Genome Biology, Adam Mickiewicz University in Poznan, 61-614 Poznan, Poland.

[3]To whom correspondence should be addressed. Email: irh25@cam.ac.uk.

This article contains supporting information online at www.pnas.org/lookup/suppl/doi:10.1073/pnas.1713071115/-/DCSupplemental.

Published online February 20, 2018.

the MLH1/MLH3 MutL-related heterodimer (1, 10) (*SI Appendix*, Fig. S1*A*). Within the ZMM pathway, the *HEI10* E3 ligase gene shows dosage sensitivity, with additional copies being sufficient to increase crossovers throughout euchromatin (13). Approximately 15% of crossovers in plants do not show interference and are known as class II, which form by a different MUS81-dependent pathway (1).

From cytological measurement of *Arabidopsis* DSB-associated foci (e.g., γH2A.X, RAD51, and DMC1) along meiotic chromosomes, it is estimated that between 100 and 200 breaks initiate per nucleus (14–16). However, only ∼10 crossovers typically form throughout the genome (17–20), indicating that anticrossovers pathways prevent maturation of the majority of initiation events into crossovers (1). Indeed, genetic analysis has identified at least three distinct anticrossovers pathways in *Arabidopsis*: (*i*) the FANCM DNA helicase and MHF1 and MHF2 cofactors (21–23), (*ii*) the AAA-ATPase FIDGETIN-LIKE1 (24), and (*iii*) the RTR complex of RECQ4A, RECQ4B DNA helicases, TOPOISOMERASE3α, and RMI1 (25–29) (*SI Appendix*, Fig. S1*A*). For example, *recq4a recq4b* mutants show highly elevated noninterfering crossovers when assayed in specific intervals (26) (*SI Appendix*, Fig. S1*A*). This is thought to primarily result from a failure to dissolve interhomolog strand invasion events, which are alternatively repaired by the noninterfering crossover pathway(s) (21, 24, 26). As combining mutations between these pathways, for example *fancm figl1*, led to additive crossover increases, they reflect parallel mechanisms (24). Hence, during meiosis, competing pathways act on SPO11-dependent DSBs to balance crossover and noncrossover repair outcomes (*SI Appendix*, Fig. S1*A*).

In this work, we explore the functional relationship between ZMM procrossover and RECQ4 anticrossovers meiotic recombination pathways. Using a combination of increased *HEI10* dosage and *recq4a recq4b* mutations, we observe a massive, additive increase in crossover frequency throughout the chromosome arms. Surprisingly, we observe that increased *HEI10* dosage (hereafter referred to as *HEI10*) causes increased crossover coincidence, indicating an effect on interference. We show that *HEI10* and *recq4a recq4b* crossover increases are biased toward regions of low interhomolog divergence that are distal from centromeric heterochromatin. Hence, both genetic and epigenetic information likely constrain the activity of meiotic recombination pathways.

Combination of *HEI10* and *recq4a recq4b* Massively Elevates Crossover Frequency

Crossover increases in *HEI10* and *recq4a recq4b* represent mechanistically distinct effects via class I and class II crossover repair pathways (*SI Appendix*, Fig. S1*A*). We therefore sought to test whether combining these genetic backgrounds would cause further increases in crossover frequency. We previously showed that transgenic line "*C2*," which carries additional *HEI10* copies, shows an approximately two-fold increase in crossovers genome-wide, compared with wild type (13) (*SI Appendix*, Table S1). We crossed *HEI10* line *C2* to *recq4a recq4b* double mutants, in the Col genetic background (13, 26, 28) (*SI Appendix*, Fig. S1*B*). A previous genetic screen isolated an EMS allele of *recq4a* in Ler (26). As Ler carries a natural premature stop codon in *recq4b* (26), this provides a *recq4a recq4b* double mutant in Ler (*SI Appendix*, Fig. S1*B*). These lines were crossed and F_1 progeny identified that were heterozygous for Col/Ler polymorphisms, *recq4a recq4b* homozygous, and with or without additional *HEI10* copies (*SI Appendix*, Fig. S1*B*). These F_1 plants were then used to generate Col/Ler F_2 for crossover analysis (*SI Appendix*, Fig. S1*B*).

During crossing, we maintained the *420* FTL crossover reporter within our lines, which allows measurement of genetic distance in a ∼5.1-Mb subtelomeric region on chromosome 3 (30, 31) (Fig. 1*A* and *SI Appendix*, Fig. S1*B* and Table S2). This showed that *HEI10*, *recq4a recq4b*, and *HEI10 recq4a recq4b* all significantly increase *420* crossover frequency in Col/Ler hybrid backgrounds, by 2.7, 3.3, and 3.7-fold, respectively (χ^2 test, $P = 2.73 \times 10^{-175}$, $P = 4.92 \times 10^{-212}$ and $P = 2.80 \times 10^{-226}$) (Fig. 1*A* and *SI Appendix*, Table S2). However, it is notable that *420* genetic distance reached 47 cM in *HEI10 recq4a recq4b*, which is close to the maximum

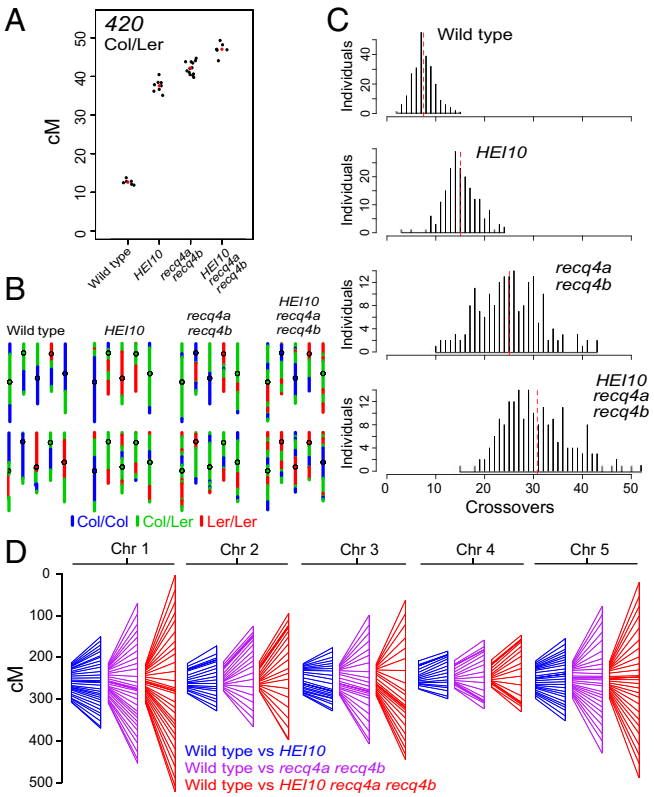

Fig. 1. Combination of *HEI10* and *recq4a recq4b* massively increases meiotic crossover frequency. (*A*) The *420* genetic distance (in centimorgans) was measured during breeding of the *HEI10* and *recq4a recq4b* populations. All samples were Col/Ler heterozygous. Replicate measurements are shown as black dots and mean values as red dots. The *HEI10* data were previously reported (13). (*B*) Chromosomal genotypes are shown for two representative individuals from the wild type, *HEI10*, *recq4a recq4b*, and *HEI10 recq4a recq4b* F_2 populations. The five *Arabidopsis* chromosomes are depicted and color coded according to Col/Col (blue), Col/Ler (green), or Ler/Ler (red) genotypes. Centromere positions are indicated by black circles. (*C*) Histograms showing the frequency of F_2 individuals containing different crossover numbers in each population, with the mean value indicated by the horizontal dotted red lines. (*D*) Genetic maps (in centimorgans) shown for each chromosome for *HEI10* (blue), *recq4a recq4b* (magenta), and *HEI10 recq4a recq4b* (red). Each map is shown alongside the wild-type map (*Left*), and markers between the maps are connected.

observable recombination frequency for linked markers (50 cM) (Fig. 1*A* and *SI Appendix*, Table S2). Therefore, we next sought to use genotyping by sequencing (GBS) to generate genome-wide, high-resolution maps of crossovers in these backgrounds.

We sequenced genomic DNA from between 191 and 245 Col/Ler F_2 progeny derived from wild type, *recq4a recq4b*, and *HEI10 recq4a recq4b* F_1 parents, and compared them with a previously described *HEI10* F_2 population (13) (*SI Appendix*, Figs. S1–S6 and Tables S1 and S3). We observed that *recq4a recq4b* caused 3.3-fold more crossovers genome-wide (25 crossovers/F_2 individual, 95% confidence interval ±0.93), compared with wild type (7.5 crossovers/F_2, 95% confidence interval ±0.28), which is greater than the twofold increase previously seen in *HEI10* (15.1 crossovers/F_2, 95% confidence interval ±0.49) (13) (Fig. 1 *B–D* and *SI Appendix*, Table S1). If the *HEI10* and *recq4a recq4b* crossover increases combined in a purely additive manner, then we would expect to see wild-type crossovers plus the sum of the *HEI10* and *recq4a recq4b* crossover differentials in *HEI10 recq4a recq4b*, equivalent to 7.5 + 7.6 + 17.4 = 32.5 crossovers/F_2. Indeed, this was similar to the observed value for *HEI10 recq4a recq4b* of 30.8 crossovers/F_2 (95% confidence interval ±0.93) (Fig. 1 *B–D* and *SI Appendix*, Table S1). For all populations, the physically largest chromosomes

had the longest genetic maps (Fig. 1*D* and *SI Appendix*, Fig. S7). Together these data show that crossover elevations caused by increased *HEI10* dosage and loss of the *RECQ4A RECQ4B* anticrossovers helicases combine in an additive manner, consistent with class I and class II crossover pathways being independent in *Arabidopsis*.

To assess whether elevated crossover frequency caused by *HEI10* and *recq4a recq4b* were associated with changes to fertility, we performed Alexander staining of pollen and scored the proportion of viable and inviable grains. Compared with wild type, *HEI10 recq4a recq4b* showed significantly higher pollen inviability ($P = 6.3 \times 10^{-4}$), whereas *HEI10* and *recq4a recq4b* were not significantly different (pairwise *t* tests were performed with correction for multiple testing) (*SI Appendix*, Fig. S8*A* and Table S4). We also measured seed set and observed that average seed number per silique in *HEI10* ($P = 1.4 \times 10^{-4}$), *recq4a recq4b* ($P = 3.7 \times 10^{-5}$), and *HEI10 recq4a recq4b* ($P = 1.8 \times 10^{-8}$) were significantly reduced compared with wild type (*SI Appendix*, Fig. S8*B* and Table S5), with the greatest reduction in *HEI10 recq4a recq4b*. Although elevated levels of meiotic crossover associate with significant reductions in fertility in these backgrounds, appreciable seed set is still observed compared with wild type in *HEI10* (94% of wild type), *recq4a recq4b* (95%), and *HEI10 recq4a recq4b* (71%) (*SI Appendix*, Fig. S8*B* and Table S5).

To investigate whether the increased crossovers observed in *HEI10*, *recq4a recq4b*, and *HEI10 recq4a recq4b* arise from additional DSBs, or at the expense of other types of repair, we measured meiotic DSB levels by immunostaining for RAD51 (a RecA homolog that mediates strand invasion) and ASY1 (a HORMA domain protein which forms part of the meiotic chromosome axis). Quantification of axis-associated RAD51 foci at leptotene, zygotene, and pachytene stages showed no significant differences between wild type and *HEI10*, *recq4a recq4b*, or *HEI10 recq4a recq4b* (*SI Appendix*, Fig. S9 and Tables S6–S8). This indicates that recombination changes in *HEI10* and *recq4a recq4b* do not feedback to cause a significant change to DSB foci during *Arabidopsis* meiosis.

Crossover Coincidence Increases in *HEI10* and *recq4a recq4b*

Underdispersion of crossover numbers per meiosis occurs due to the action of crossover interference (1, 10, 32), causing an excess of values close to the mean. Consistently, we observe that the distribution of crossovers per wild-type F_2 individual is significantly non-Poisson (goodness-of-fit test for Poisson distribution, $P = 0.012$) (Fig. 2*A*). Observed frequencies are plotted as bars (gray) originating from the fitted frequencies (red line), such that gray bars lying above or below zero on the *y* axis represent deviation from the Poisson expectation (Fig. 2*A*). Crossover distributions per individual in *HEI10*, *recq4a recq4b*, and *HEI10 recq4a recq4b* were also significantly non-Poisson (*HEI10* $P = 4.23 \times 10^{-3}$, *recq4a recq4b* $P = 1.85 \times 10^{-5}$ and *HEI10 recq4a recq4b* $P = 0.0174$). However, the high recombination populations also showed significantly greater variation in crossover numbers compared with wild type (Brown–Levene test, *HEI10* $P = 1.08 \times 10^{-6}$, *recq4a recq4b* $P \leq 2.2 \times 10^{-16}$, *HEI10 recq4a recq4b* $P \leq 2.2 \times 10^{-16}$) (Fig. 2*A* and *SI Appendix*, Table S1). We therefore sought to examine the distributions of crossovers within the GBS data in more detail, with respect to interevent spacing.

The analysis of F_2 individuals resulting from two independent meioses does not allow us to distinguish between genuine (*cis*) DCOs, which occurred in a single meiosis, or apparent (*trans*) DCOs, which are the result of a single crossover from two different meioses, which combined to form a given F_2 individual (Fig. 2*B*). However, we adopted a hypothesis testing approach to ask whether observed crossover distances differed significantly from those expected from a Poisson distribution. We considered each F_2 individual separately, identified chromosomes with two or more crossovers, and calculated the distance between them. For each individual and chromosome, the same number of randomly chosen positions was used to generate a matched set of distances (Fig. 2*B*). Consistent with the action of interference, wild-type distances were significantly greater than the corresponding random distances (mean = 8.72 Mb vs. 6.91 Mb, Mann–Whitney Wilcoxon test $P = 1.39 \times 10^{-11}$). In *HEI10* the distances were substantially reduced compared with wild type, but were still significantly greater than random (mean = 6.06 Mb vs. 5.15 Mb, Mann–Whitney Wilcoxon test $P = 3.88 \times 10^{-12}$) (Fig. 2*B*). However, in both *recq4a recq4b* (mean = 3.84 Mb vs. 3.45 Mb, Mann–Whitney Wilcoxon test $P = 0.08$) and *HEI10 recq4a recq4b* (mean = 3.30 Mb vs. 3.09 Mb, Mann–Whitney Wilcoxon test $P = 0.257$) populations, the observed distances were not significantly different from random (Fig. 2*B*). This is expected as increased class II crossovers caused by *recq4a recq4b* are randomly distributed (26). We also observed that the differential between observed and randomly generated distances was less in *HEI10* (1.176×), compared with wild type (1.262×). Therefore, we sought to further investigate crossover interference in *HEI10* compared with wild type.

To measure crossover interference in wild type and *HEI10* we used three-color FTL analysis, with the adjacent *I3b* and *I3c* intervals. *I3bc* allows measurement of crossover frequency in a subtelomeric region of chromosome 3 (31, 33) (*I3bc* is located within the *420* FTL interval described earlier) (Figs. 1*A* and 2*C*). We used flow cytometry to measure inheritance of pollen fluorescence in wild type and *HEI10* and calculate *I3b* and *I3c* genetic distances (Fig. 2*C* and *SI Appendix*, Tables S9 and S10). Both *I3b* and *I3c* showed a significant increase in crossover frequency in *HEI10*, consistent with our previous *420* measurements (χ^2 test both $P \leq 2.2 \times 10^{-16}$) (Figs. 1*A* and 2*C* and *SI Appendix*, Tables S9 and S10). *I3b* and *I3c* genetic distances were used to estimate the number of DCO pollen expected in the absence of interference, using the

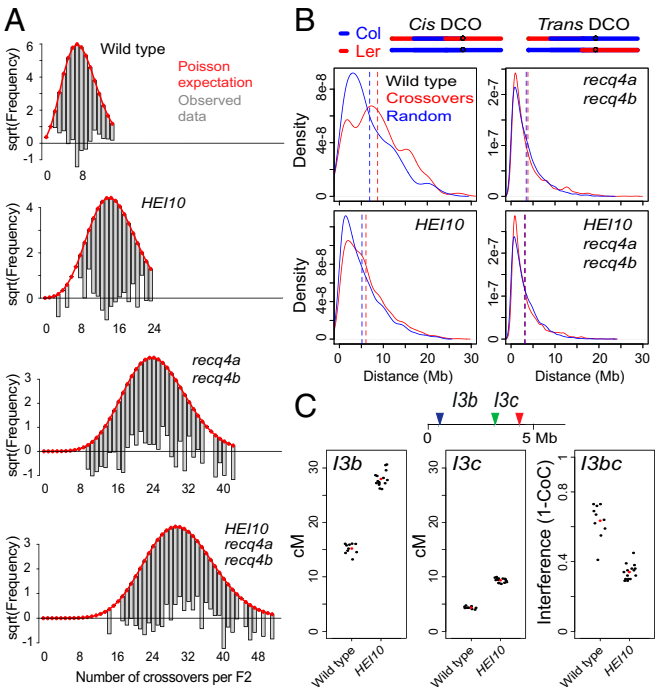

Fig. 2. Decreased crossover interference in *HEI10* and *recq4a recq4b*. (*A*) Plots of the square root of the frequency of total crossovers per F_2 individual in wild type, *HEI10*, *recq4a recq4b*, and *HEI10 recq4a recq4b* populations, generated using the R package goodfit. The expected Poisson distribution is plotted in red, with the observed data below. Deviation from the Poisson expectation is shown by the gray bars (observed data) falling either above or below the zero value on the *y* axis. (*B*) The *Upper* diagram illustrates genuine (*cis*) versus apparent (*trans*) double crossovers detected in F_2 genotyping data. Kernel density estimates are plotted for observed distances between crossovers (red) and the same number of randomly chosen distances (blue), for the indicated genotypes. The vertical dotted lines indicate mean values. (*C*) *I3b* and *I3c* genetic distances in wild type and *HEI10*, and crossover interference (1 – CoC) between the *I3b* and *I3c* intervals. Replicate measurements are shown by black dots and mean values by red dots.

formula: expected DCOs = (*I3b* cM/100) × (*I3c* cM/100) × total pollen number. The ratio of "observed DCOs" to "expected DCOs" gives the coefficient of coincidence (CoC), and interference is calculated as 1 – CoC, such that zero indicates an absence of interference (31, 33) (Fig. 2*C* and *SI Appendix*, Tables S9 and S10). *I3bc* interference (1 – CoC) significantly decreased from 0.64 in wild type to 0.34 in *HEI10* (χ^2 test $P \leq 2.2 \times 10^{-16}$) (Fig. 2*C* and *SI Appendix*, Tables S9 and S10). These experiments reveal that although *HEI10* functions in the interfering ZMM pathway, higher *HEI10* dosage causes increased crossover coincidence compared with wild type, although not to the degree observed in *recq4a recq4b* (25) (Fig. 2*B*).

Crossover, Interhomolog Divergence, and DNA Methylation Landscapes

We next sought to analyze crossover distributions along the chromosomes and relate these patterns to other aspects of genome organization (Fig. 3). On average, 7.5 crossovers were observed per wild-type F_2 individual, 5.6 of which occurred in the chromosome arms and 1.9 in the pericentromeric heterochromatin (*SI Appendix*, Fig. S10 and Table S11). In *HEI10*, *recq4a recq4b*, and *HEI10 recq4a recq4b*, crossovers in the arms increased 2.3, 4.1, and 5-fold, respectively (5.6, 12.9, 23, and 28 crossovers), whereas the pericentromere increases of 1.1, 1.1, and 1.5-fold, respectively (1.9, 2.1, 2.0, and 2.7 crossovers), were considerably lower (*SI Appendix*, Fig. S10 and Table S11). Consistent with previous observations (13, 34), we observed that despite massive crossover increases throughout the chromosome arms, *HEI10*, *recq4a recq4b*, and *HEI10 recq4a recq4b* maintain suppression of recombination within the centromeric regions (Fig. 3). We also observed that a subtelomeric region on the long arm of chromosome 4 showed suppression of crossovers, specifically in the *recq4a recq4b* and *HEI10 recq4a recq4b* populations (Fig. 3). This may reflect a lineage-specific sequence rearrangement, such as an inversion, shared among the *recq4a recq4b* backgrounds.

We hypothesized that genetic and epigenetic factors could contribute to the observed telomeric bias in crossover increases. Therefore, we compared recombination to patterns of Col/Ler interhomolog divergence (35) (i.e., heterozygosity) and DNA cytosine methylation (36). Within the chromosome arms, we observed that wild-type crossovers showed a positive relationship with divergence (all values were calculated in 300-kb adjacent windows, Pearson's $r = 0.564$ $P < 2.2 \times 10^{-16}$), which is reminiscent of correlations previously observed between historical recombination and sequence diversity (31) (Figs. 3 and 4). In contrast, opposite negative correlations were seen between *HEI10* ($r = -0.640$ $P < 2.2 \times 10^{-16}$), *recq4a recq4b* ($r = -0.805$ $P < 2.2 \times 10^{-16}$) and *HEI10 recq4a recq4b* ($r = -0.810$ $P < 2.2 \times 10^{-16}$) crossovers and Col/Ler SNP divergence (Figs. 3 and 4). This indicates that the crossover elevations seen in *HEI10 recq4a recq4b* are biased toward the least polymorphic regions of the chromosomes. Hence, while the class II repair pathway that is active in *recq4a recq4b* is not completely inhibited by heterozygosity, it shows a preference for regions of lower interhomolog divergence.

To further investigate the relationship between crossovers and structural genetic variation, we compared crossovers with a set of 47 Col/Ler inversions (35), which have a mean length of 33.8 kb and comprise 1.59 Mb in total. For each genotype, we counted overlap of crossovers with the inversions and compared inversion overlap with a matched set of randomly chosen intervals with the same widths. In total, we observed that 8 of 15,425 crossovers overlapped the inversions, which was significantly fewer than the 189 overlaps observed for random (χ^2 test $P < 2.2 \times 10^{-16}$). This is consistent with Col/Ler inversions potently inhibiting crossovers (35). We also note that zero crossovers overlapped the 1.17 Mb heterochromatic knob inversion on chromosome 4 (37). The densely DNA methylated centromeric regions were strongly

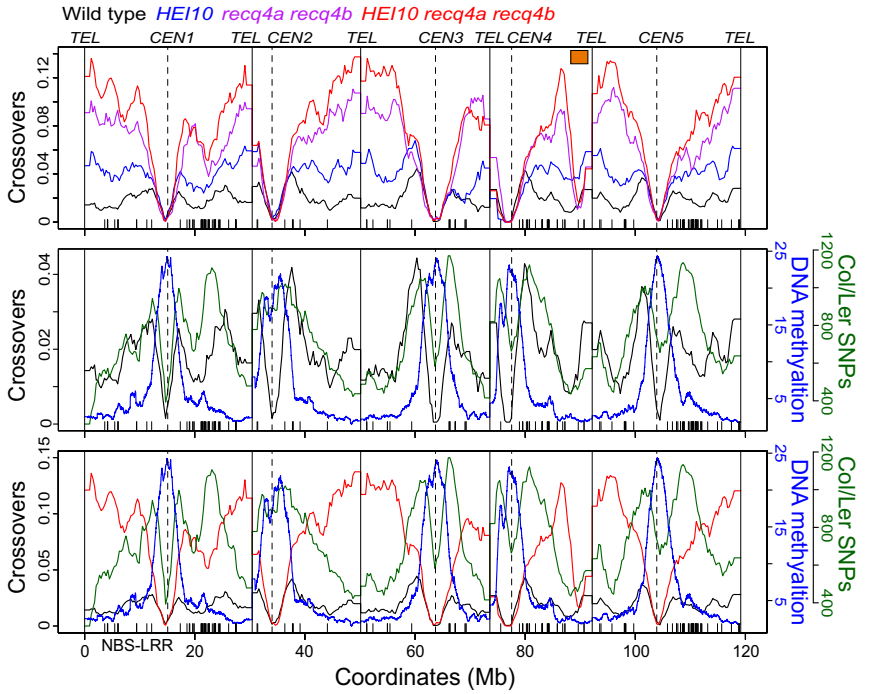

Fig. 3. Genomic landscapes of crossover frequency, interhomolog divergence, and DNA methylation. (*Upper*) Plots of crossover frequency (crossovers per 300 kb, normalized by the number of F_2 individuals analyzed) measured in wild type (black), *HEI10* (blue) (13), *recq4a recq4b* (purple), and *HEI10 recq4a recq4b* (red). The five chromosomes are plotted on a continuous *x* axis, with the positions of telomeres (*TEL*) and centromeres (*CEN*) indicated by vertical lines. The position of NBS-LRR resistance gene homologs are indicated by the *x* axis ticks. The putative location of an inversion in the *recq4a recq4b*-derived populations is also indicated by the *Inset* orange rectangle. (*Middle*) As for *Upper*, but showing wild-type crossover frequency (black) plotted against Col/Ler SNPs (SNPs/300 kb, green) (35) and DNA methylation (% per 10 kb, blue) (36). (*Lower*) As for *Middle*, but showing both wild-type (black) and *HEI10 recq4a recq4b* (red) crossover frequency using a greater *y* axis range.

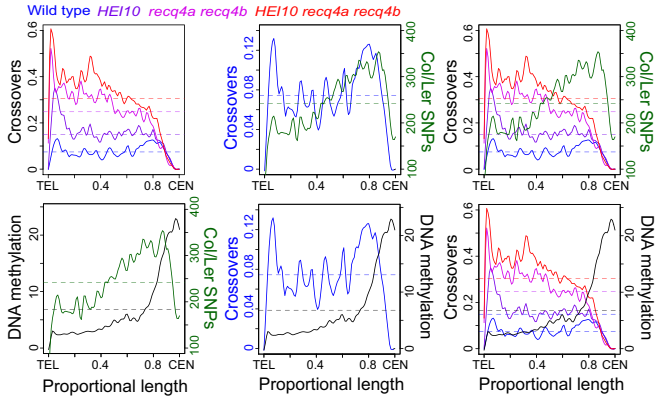

Fig. 4. Crossover frequency, interhomolog divergence, and DNA methylation along telomere–centromere chromosome axes. Analysis of crossover frequency in wild type (blue), *HEI10* (purple), *recq4a recq4b* (magenta), *HEI10 recq4a recq4b* (red), Col/Ler SNPs (green) (35), and DNA methylation (black) (36), analyzed along the proportional length of all chromosome arms, orientated from telomeres (*TEL*) to centromeres (*CEN*).

crossover suppressed in all populations, consistent with heterochromatin inhibiting meiotic recombination (36) (Figs. 3 and 4). Crossovers were negatively correlated with DNA methylation in all populations, but most strongly in the high recombination backgrounds (wild type $r = -0.233$ $P = 2.13 \times 10^{-6}$, *HEI10* $r = -0.740$ $P \leq 2.2 \times 10^{-16}$, *recq4a recq4b* $r = -0.828$ $P \leq 2.2 \times 10^{-16}$, and *HEI10 recq4a recq4b* $r = -0.810$ $P \leq 2.2 \times 10^{-16}$). Therefore, although combination of *HEI10* and *recq4a recq4b* causes a massive crossover increase, the localization of recombination appears to be constrained by both interhomolog sequence divergence and chromatin.

Discussion

We show that elevating the ZMM crossover pathway, via increased dosage of the *HEI10* meiotic E3 ligase gene, while simultaneously increasing the activity of noninterfering repair, via mutation of *RECQ4A* and *RECQ4B* antirecombination helicase genes, is sufficient to cause a massive increase in *Arabidopsis* meiotic crossovers. This is consistent with class I and class II acting as independent crossover repair pathways in *Arabidopsis*. HEI10 is a highly conserved ubiquitin/SUMO E3 ligase with unknown targets during *Arabidopsis* meiosis, which may include other ZMM factors (1, 10, 38). In plants, HEI10 associates with paired homologous chromosomes throughout meiotic prophase, showing gradual restriction to a small number of foci that correspond to crossover locations (39, 40). We propose that HEI10 acts to quantitatively promote ZMM pathway crossover repair at recombination sites via SUMO or ubiquitin transfer. Unexpectedly, we show that increased *HEI10* dosage causes higher crossover coincidence and therefore a decrease in genetic interference. Crossover interference has been modeled as a mechanical force, thought to be transmitted via the meiotic chromosome axis and/or synaptonemal complex (SC) (41). Therefore, HEI10 may modify recombination factors at repair foci and decrease their sensitivity to the interference signal, thereby increasing the likelihood of ZMM-dependent crossover designation. Alternatively HEI10 may alter transmission of the interference signal per se, for example, if components of the axis or SC are SUMO/ubiquitin targets.

The RECQ4 helicases have biochemically characterized activities in (*i*) disassembly of D loops and (*ii*) decatenation of dHJs (42–45), and thus can promote noncrossover outcomes at multiple recombination steps poststrand invasion. In the *recq4a recq4b* mutant, it is likely that unrepaired joint molecules persist, which are instead repaired as noninterfering class II crossovers (26). We show that combination of genetic backgrounds that increase class I and class II crossovers is sufficient to cause a massive and additive recombination increase from 7.5 to 31 crossovers per *Arabidopsis* F_2 individual. However, given that ~100–200 DSB foci have been cytogenetically observed in *Arabidopsis*, there likely remains the capacity for further crossover increases (14–16). As the *Arabidopsis* anticrossovers pathways do not show complete redundancy (21, 24, 26, 46), combination of mutations in the *FANCM*, *RECQ4A-RECQ4B*, and *FIGL1* pathways can cause further crossover increases (34). Furthermore, the *Arabidopsis* MSH2 MutS homolog acts to suppress crossovers specifically when homologous chromosomes are polymorphic (47), and therefore introduction of *msh2* mutations may further increase recombination in hybrids. The use of *msh2* is attractive, as it may reduce the bias against crossovers observed in divergent regions in *HEI10 recq4a recq4b*.

It is notable that the effects of *HEI10* and *recq4a recq4b* are most potent at increasing crossovers in euchromatin. Therefore, in crop species with large heterochromatic regions, these strategies may increase recombination most strongly in subtelomeric euchromatin (2). Interestingly, in maize, <3% of the genome has been identified as nucleosome depleted, recombination active, and contributing to the majority of heritable variation (48), meaning that increased crossovers in these regions would likely influence inheritance of key traits. To unlock recombination in the pericentromeric regions, modification of epigenetic information may be required. However, as plant heterochromatin is maintained by multiple interacting systems of epigenetic marks, including DNA methylation, H3K9me2, H3K27me1, and H2A.W (49), these varying modifications may have differentiated functions in control of meiotic recombination (36, 50, 51). Importantly, the balance of heterochromatic systems is also known to vary between species. For example, islands of CHH DNA methylation occur adjacent to active genes in maize, which are not evident in *Arabidopsis* (52). In conclusion, advanced tailoring of genetic backgrounds may further bias meiotic DSB repair to crossover fates, which has the potential to accelerate crop breeding and improvement.

Materials and Methods

Plant Materials. *Arabidopsis* lines used in this study were the Col *HEI10* line *C2* (13), Col *recq4a-4* (N419423) (28), Col *recq4b-2* (N511130) (28), and Ler *recq4a* line (W387*) (26). Genotyping of *recq4a-4* was performed by PCR amplification using recq4a-F and recq4-wt-R oligonucleotides for wild type and recq4a-F and recq4-mut-R for *recq4a-4*. Genotyping of *recq4b-2* was carried out by PCR amplification using recq4b-wt-F and R oligonucleotides for wild type and recq4b-mut-F and R oligonucleotides for *recq4b-2*. Genotyping of *recq4a* mutation in Ler was performed by PCR amplification using recq4a-Ler-F and R oligonucleotides and subsequent digestion of the PCR products by ScrFI restriction enzyme, which yields ~160 bp products for wild type and ~180 bp products for *recq4a*. The presence of *HEI10* transgene was tested by PCR amplification using HEI10-F and HEI10-R oligonucleotides. Oligonucleotide sequences are provided in *SI Appendix*, Table S12.

Measurement of Crossover Frequency Using Fluorescent Tagged Lines. The *420* genetic distance was measured using microscopic analysis of seed fluorescence, as described (30, 31). *I3bc* genetic distances and coefficient of coincidence were measured using fluorescent pollen and flow cytometry, as described (31). Statistical analysis of FTL crossover frequency and interference measurements were performed as described (13, 31).

Immunocytological Analysis. Chromosome spreads of *Arabidopsis* pollen mother cells and immunostaining of ASY1 and RAD51 were prepared as described (53). Individual cells were acquired as Z stacks of 10 optical sections of 0.2 μM each. The maximum intensity projection for each cell was rendered using ImageJ, and RAD51 foci associated with the meiotic chromosome axis were counted manually. The following antibodies were used: α-ASY1 (53) (rat, 1:300 dilution) and α-RAD51 (54) (rabbit, 1:300 dilution). Microscopy was conducted using a DeltaVision Personal DV microscope (Applied Precision/GE Healthcare) equipped with a CDD Coolsnap HQ2 camera (Photometrics). Image capture was performed using SoftWoRx software version 5.5 (Applied Precision/GE Healthcare).

Genotyping by Sequencing. Ler genomic DNA was sequenced and reads were aligned to the TAIR10 genome assembly using Bowtie2. Variant sites were called using SAMtools and BCFtools. Sites were filtered to remove those with qualities <100 and >2.5× mean coverage and repeat masked (15). A set of 481,252 SNPs (mean spacing = 248 bp) were selected for analysis using the TIGER pipeline (36, 55). DNA was extracted from F_2 plants and used to generate GBS libraries, and crossovers were identified between "complete" SNP positions.

Across all datasets, crossovers were resolved to a mean distance of 1,409 bp. FastQ sequencing data files are available from ArrayExpress accession E-MTAB-5949.

To generate genetic maps, GBS genotypes from each library were used to call "marker" genotypes at 1-Mb intervals. These genotypes were used with the R package Rqtl to generate genetic maps using the Haldane mapping function. The R package goodfit was used to compare observed crossover numbers per individual to the Poisson expectation. For analysis of crossover locations, we used a genetic definition of the centromeres as the contiguous regions surrounding the centromeric assembly gaps that show an absence of crossovers in wild type (56). We defined the surrounding regions with higher than average DNA methylation as the pericentromeres (36). The chromosome arms were defined as the remainder of the genome. The *HEI10* line *C2* contains a translocation between chromosomes 3 (~159,900 bp) and 4 (~20,780,000) associated with the *HEI10* transgene, which results in false crossover calls at these locations. For this reason, 74 crossovers at these positions were masked from further analysis.

ACKNOWLEDGMENTS. We thank Gregory Copenhaver (University of North Carolina, Chapel Hill) for *I3bc*, Avraham Levy (Weizmann Institute) for *420*, Chris Franklin (University of Birmingham) for ASY1 and RAD51 antibodies, and the Gurdon Institute Imaging Facility for access to microscopes. This work was supported by grants from the Biotechnology and Biological Sciences Research Council (BBSRC) (BB/L006847/1), BBSRC-Meiogenix IPA (BB/N007557/1), European Research Area Network for Coodinating Action in Plant Sciences/BBSRC "DeCOP" (BB/M004937/1), Marie-Curie "COMREC" network FP7 ITN-606956, European Research Council (SynthHotspot CoG), the Gatsby Charitable Foundation (GAT2962), a Royal Society University Research Fellowship, and the Bettencourt Schueller Foundation.

1. Mercier R, Mézard C, Jenczewski E, Macaisne N, Grelon M (2015) The molecular biology of meiosis in plants. *Annu Rev Plant Biol* 66:297–327.
2. Higgins JD, Osman K, Jones GH, Franklin FCH (2014) Factors underlying restricted crossover localization in barley meiosis. *Annu Rev Genet* 48:29–47.
3. Keeney S, Kleckner N (1995) Covalent protein-DNA complexes at the 5′ strand termini of meiosis-specific double-strand breaks in yeast. *Proc Natl Acad Sci USA* 92:11274–11278.
4. Neale MJ, Pan J, Keeney S (2005) Endonucleolytic processing of covalent protein-linked DNA double-strand breaks. *Nature* 436:1053–1057.
5. Cannavo E, Cejka P (2014) Sae2 promotes dsDNA endonuclease activity within Mre11-Rad50-Xrs2 to resect DNA breaks. *Nature* 514:122–125.
6. Garcia V, Phelps SEL, Gray S, Neale MJ (2011) Bidirectional resection of DNA double-strand breaks by Mre11 and Exo1. *Nature* 479:241–244.
7. Zakharyevich K, et al. (2010) Temporally and biochemically distinct activities of Exo1 during meiosis: Double-strand break resection and resolution of double Holliday junctions. *Mol Cell* 40:1001–1015.
8. Mimitou EP, Yamada S, Keeney S (2017) A global view of meiotic double-strand break end resection. *Science* 355:40–45.
9. Brown MS, Bishop DK (2014) DNA strand exchange and RecA homologs in meiosis. *Cold Spring Harb Perspect Biol* 7:a016659.
10. Hunter N (2015) Meiotic recombination: The essence of heredity. *Cold Spring Harb Perspect Biol* 7:a016618.
11. Copenhaver GP, Housworth EA, Stahl FW (2002) Crossover interference in Arabidopsis. *Genetics* 160:1631–1639.
12. Mercier R, et al. (2005) Two meiotic crossover classes cohabit in Arabidopsis: One is dependent on MER3,whereas the other one is not. *Curr Biol* 15:692–701.
13. Ziolkowski PA, et al. (2017) Natural variation and dosage of the HEI10 meiotic E3 ligase control *Arabidopsis* crossover recombination. *Genes Dev* 31:306–317.
14. Chelysheva L, et al. (2010) An easy protocol for studying chromatin and recombination protein dynamics during Arabidopsis thaliana meiosis: Immunodetection of cohesins, histones and MLH1. *Cytogenet Genome Res* 129:143–153.
15. Choi K, et al. (2013) Arabidopsis meiotic crossover hot spots overlap with H2A.Z nucleosomes at gene promoters. *Nat Genet* 45:1327–1336.
16. Ferdous M, et al. (2012) Inter-homolog crossing-over and synapsis in Arabidopsis meiosis are dependent on the chromosome axis protein AtASY3. *PLoS Genet* 8: e1002507.
17. Wijnker E, et al. (2013) The genomic landscape of meiotic crossovers and gene conversions in Arabidopsis thaliana. *eLife* 2:e01426.
18. Copenhaver GP, Browne WE, Preuss D (1998) Assaying genome-wide recombination and centromere functions with Arabidopsis tetrads. *Proc Natl Acad Sci USA* 95: 247–252.
19. Salomé PA, et al. (2012) The recombination landscape in Arabidopsis thaliana F2 populations. *Heredity (Edinb)* 108:447–455.
20. Giraut L, et al. (2011) Genome-wide crossover distribution in Arabidopsis thaliana meiosis reveals sex-specific patterns along chromosomes. *PLoS Genet* 7:e1002354.
21. Crismani W, et al. (2012) FANCM limits meiotic crossovers. *Science* 336:1588–1590.
22. Girard C, et al. (2014) FANCM-associated proteins MHF1 and MHF2, but not the other Fanconi anemia factors, limit meiotic crossovers. *Nucleic Acids Res* 42:9087–9095.
23. Knoll A, et al. (2012) The Fanconi anemia ortholog FANCM ensures ordered homologous recombination in both somatic and meiotic cells in Arabidopsis. *Plant Cell* 24: 1448–1464.
24. Girard C, et al. (2015) AAA-ATPase FIDGETIN-LIKE 1 and helicase FANCM antagonize meiotic crossovers by distinct mechanisms. *PLoS Genet* 11:e1005369, and erratum (2015) 11:e1005448.
25. Séguéla-Arnaud M, et al. (2016) RMI1 and TOP3α limit meiotic CO formation through their C-terminal domains. *Nucleic Acids Res* 287:gkw1210.
26. Séguéla-Arnaud M, et al. (2015) Multiple mechanisms limit meiotic crossovers: TOP3α and two BLM homologs antagonize crossovers in parallel to FANCM. *Proc Natl Acad Sci USA* 112:4713–4718.
27. Bonnet S, Knoll A, Hartung F, Puchta H (2013) Different functions for the domains of the Arabidopsis thaliana RMI1 protein in DNA cross-link repair, somatic and meiotic recombination. *Nucleic Acids Res* 41:9349–9360.
28. Hartung F, Suer S, Puchta H (2007) Two closely related RecQ helicases have antagonistic roles in homologous recombination and DNA repair in Arabidopsis thaliana. *Proc Natl Acad Sci USA* 104:18836–18841.
29. Higgins JD, Ferdous M, Osman K, Franklin FCH (2011) The RecQ helicase AtRECQ4A is required to remove inter-chromosomal telomeric connections that arise during meiotic recombination in Arabidopsis. *Plant J* 65:492–502.
30. Melamed-Bessudo C, Yehuda E, Stuitje AR, Levy AA (2005) A new seed-based assay for meiotic recombination in Arabidopsis thaliana. *Plant J* 43:458–466.
31. Ziolkowski PA, et al. (2015) Juxtaposition of heterozygous and homozygous regions causes reciprocal crossover remodelling via interference during Arabidopsis meiosis. *eLife* 4:e03708.
32. Jones GH, Franklin FCH (2006) Meiotic crossing-over: Obligation and interference. *Cell* 126:246–248.
33. Berchowitz LE, Copenhaver GP (2008) Fluorescent Arabidopsis tetrads: A visual assay for quickly developing large crossover and crossover interference data sets. *Nat Protoc* 3:41–50.
34. Fernandes JB, Séguéla-Arnaud M, Larchevêque C, Lloyd AH, Mercier R (2017) Unleashing meiotic crossovers in hybrid plants. *Proc Natl Acad Sci USA* 115:2431–2436.
35. Zapata L, et al. (2016) Chromosome-level assembly of *Arabidopsis thaliana* Ler reveals the extent of translocation and inversion polymorphisms. *Proc Natl Acad Sci USA* 113: E4052–E4060.
36. Yelina NE, et al. (2015) DNA methylation epigenetically silences crossover hot spots and controls chromosomal domains of meiotic recombination in Arabidopsis. *Genes Dev* 29:2183–2202.
37. Fransz PF, et al. (2000) Integrated cytogenetic map of chromosome arm 4S of A. thaliana: Structural organization of heterochromatic knob and centromere region. *Cell* 100:367–376.
38. Gray S, Cohen PE (2016) Control of meiotic crossovers: From double-strand break formation to designation. *Annu Rev Genet* 50:175–210.
39. Chelysheva L, et al. (2012) The Arabidopsis HEI10 is a new ZMM protein related to Zip3. *PLoS Genet* 8:e1002799.
40. Wang K, et al. (2012) The role of rice HEI10 in the formation of meiotic crossovers. *PLoS Genet* 8:e1002809.
41. Kleckner N, et al. (2004) A mechanical basis for chromosome function. *Proc Natl Acad Sci USA* 101:12592–12597.
42. Bachrati CZ, Borts RH, Hickson ID (2006) Mobile D-loops are a preferred substrate for the Bloom's syndrome helicase. *Nucleic Acids Res* 34:2269–2279.
43. Cejka P, Plank JL, Bachrati CZ, Hickson ID, Kowalczykowski SC (2010) Rmi1 stimulates decatenation of double Holliday junctions during dissolution by Sgs1-Top3. *Nat Struct Mol Biol* 17:1377–1382.
44. Wu L, Hickson ID (2003) The Bloom's syndrome helicase suppresses crossing over during homologous recombination. *Nature* 426:870–874.
45. Hatkevich T, Sekelsky J (2017) Bloom syndrome helicase in meiosis: Pro-crossover functions of an anti-crossover protein. *BioEssays* 39:1700073.
46. Choi K, et al. (2016) Recombination rate heterogeneity within Arabidopsis disease resistance genes. *PLoS Genet* 12:e1006179.
47. Emmanuel E, Yehuda E, Melamed-Bessudo C, Avivi-Ragolsky N, Levy AA (2006) The role of AtMSH2 in homologous recombination in Arabidopsis thaliana. *EMBO Rep* 7: 100–105.
48. Rodgers-Melnick E, Vera DL, Bass HW, Buckler ES (2016) Open chromatin reveals the functional maize genome. *Proc Natl Acad Sci USA* 113:E3177–E3184.
49. Law JA, Jacobsen SE (2010) Establishing, maintaining and modifying DNA methylation patterns in plants and animals. *Nat Rev Genet* 11:204–220.
50. Choi K, et al. (2017) Nucleosomes and DNA methylation shape meiotic DSB frequency in Arabidopsis transposons and gene regulatory regions. bioRxiv:10.1101/160911.
51. Underwood CJ, et al. (2017) Epigenetic activation of meiotic recombination in Arabidopsis centromeres via loss of H3K9me2 and non-CG DNA methylation. bioRxiv: 10.1101/160929.
52. Li Q, et al. (2015) RNA-directed DNA methylation enforces boundaries between heterochromatin and euchromatin in the maize genome. *Proc Natl Acad Sci USA* 112: 14728–14733.
53. Armstrong SJ, Caryl AP, Jones GH, Franklin FCH (2002) Asy1, a protein required for meiotic chromosome synapsis, localizes to axis-associated chromatin in Arabidopsis and Brassica. *J Cell Sci* 115:3645–3655.
54. Sanchez-Moran E, Santos J-L, Jones GH, Franklin FCH (2007) ASY1 mediates AtDMC1-dependent interhomolog recombination during meiosis in Arabidopsis. *Genes Dev* 21: 2220–2233.
55. Rowan BA, Patel V, Weigel D, Schneeberger K (2015) Rapid and inexpensive whole-genome genotyping-by-sequencing for crossover localization and fine-scale genetic mapping. *G3 (Bethesda)* 5:385–398.
56. Copenhaver GP, et al. (1999) Genetic definition and sequence analysis of Arabidopsis centromeres. *Science* 286:2468–2474.